International Journal of Mass Spectrometry 377 (2015) 440–447

Contents lists available at ScienceDirect

International Journal of Mass Spectrometry

journal homepage: www.elsevier.com/locate/ijms

Halide anion binding to Gly_3, Ala_3 and Leu_3

Terrence M. Chang[a], Giel Berden[b], Jos Oomens[b,c], Evan R. Williams[a,*]

[a] Department of Chemistry, University of California, Berkeley, CA 94720-1460, United States
[b] Radboud University Nijmegen, Institute for Molecules and Materials, FELIX Facility, Toernooiveld 7, 6525 ED Nijmegen, The Netherlands
[c] Van't Hoff Institute for Molecular Sciences, University of Amsterdam, Science Park 904, 1098 XH Amsterdam, The Netherlands

ARTICLE INFO

Article history:
Received 9 January 2014
Received in revised form 27 February 2014
Accepted 28 February 2014
Available online 12 March 2014

Keywords:
Halide anion
Ion spectroscopy
Free electron laser
Infrared spectroscopy
Infrared multiple photon dissociation
Peptide

ABSTRACT

The structures of $Gly_3 \cdot X^-$, $Ala_3 \cdot X^-$ and $Leu_3 \cdot X^-$ (X = Cl, Br and I) are investigated with computational chemistry and infrared multiple-photon dissociation (IRMPD) spectroscopy. Low-energy structures calculated at the B3LYP/6-31+G** level of theory (or with the CRENBL basis set and effective core potential implemented for Br and I) for these complexes have similar structural motifs in which the halide anion binds to the peptide via hydrogen bonds at amide, amine, and/or carboxylic acid H atoms. The IRMPD spectra do not depend significantly on anion identity. Comparisons between measured spectra and those calculated for low-energy structures of each of the chloridated complexes indicate that all three complexes have similar binding motifs. These results suggest that the size of the alkyl side chain does not significantly influence how halide anions bind to these peptides. The coordination geometries of $Gly_3 \cdot X^-$ and $Ala_3 \cdot X^-$ are "inverted" compared to those for the Na^+ cationized peptides, where the peptides coordinate to Na^+ via lone pair electrons of O and N atoms. The "inversion" in structures between $Ala_3 \cdot Na^+$ and $Ala_3 \cdot X^-$ results in greater steric hindrance for some geometries of the latter. There is a subtle blue shift in the C-terminal C=O stretch frequency with increasing halide anion size for each peptide, consistent with contributions from Stark and charge transfer effects. In contrast, the N—H bends red shift with increasing halide anion size, which can only be attributed to the charge transfer effect. This is the first report of IR spectra of peptides complexed with anions, and these results provide insights into anion-peptide binding interactions.

1. Introduction

Ions and their interactions with amino acids, peptides and proteins are important in many biological processes, such as pH regulation [1,2], protein structure and complex assembly [3,4], uptake of amino acids by bacteria [5] and neuron signaling [6]. For example, Ca^{2+}-gated Cl^- channels regulate the conductance of olfactory receptors [7–10]. Investigating how ions interact with biomolecules in solution can be difficult because of the complex environment consisting of the biomolecules and ions of interest as well as ubiquitous counter ions, solvent molecules and impurities. In the gas phase, specific ion-biomolecule complexes can be isolated by mass spectrometry and probed using a wide variety of structurally informative techniques.

Information about ion-biomolecule interactions can be obtained from fragmentation [11–16], ion-mobility [17–20] and spectroscopy experiments [21–43]. Infrared multiple-photon dissociation (IRMPD) spectroscopy studies have provided detailed information about structures of many amino acids and peptides as well as their complexes with ion adducts [22–43]. The size of the cation adducts can influence how the amino acid coordinates to the ion as well as the relative stabilities between zwitterionic and nonzwitterionic forms of amino acids [30–37]. These types of studies provide a fundamental understanding of how ions interact with amino acids and affect their structures in the absence of competing effects from counterions or solvent molecules.

The interactions between anions and amino acids have been the subject of fewer studies [42–47], in contrast to the more widely investigated interactions of cations with amino acids or peptides. A zwitterionic form of Arg can be stabilized by the attachment of an excess electron [45,46] or by complexation with halide anions [42–44]. The zwitterionic form of Gly was calculated to be metastable when the dianion of oxalic or malonic

* Corresponding author. Tel.: +1 510 643 7161; fax: +1 510 742 8369.
E-mail address: erw@berkeley.edu (E.R. Williams).

http://dx.doi.org/10.1016/j.ijms.2014.02.019
1387-3806/

acid is adducted [47]. IRMPD studies of anions and amino acids have been reported [42,43] and provide valuable insights into the spectroscopy of these complexes. However, more complicated interactions between anions and peptides have yet to be characterized spectroscopically.

Here, we report the first IRMPD spectra of $Gly_3 \cdot X^-$, $Ala_3 \cdot X^-$ and $Leu_3 \cdot X^-$, X = Cl, Br and I, in combination with calculated low-energy structures and their relative Gibbs free energies (298 K). The relative energies as well as comparisons between the IRMPD spectra and the simulated spectra of low-energy structures are used to determine the most stable conformers. These results provide useful insight into how the size of alkyl side-chains affect the structure of peptides with anion adducts and are the first reported spectra of anions bound to peptides.

2. Computational and experimental methods

2.1. Computational

Separate conformational searches for $Gly_3 \cdot Cl^-$ and $Ala_3 \cdot Cl^-$ were performed using Macromodel v. 9.8 with MMFFs to generate at least 6000 low-energy structures. These initial geometries were grouped into families based on similar backbone and hydrogen-bonding motifs, and a representative structure from each family was selected for quantum mechanical optimization using Q-Chem v. 4.0 [48] at the B3LYP/6-31+G** level of theory. Zero-point energies and 298 K enthalpies and entropies were computed using unscaled harmonic oscillator vibrational frequencies calculated at the same level of theory. Initial geometries for $Leu_3 \cdot Cl^-$ were generated by side chain substitution for the three lowest-energy structures of $Ala_3 \cdot Cl^-$. Quantum mechanical optimization for $Leu_3 \cdot Cl^-$ was also done at the B3LYP/6-31+G** level of theory. Low-energy structures for $Gly_3 \cdot Cl^-$, $Ala_3 \cdot Cl^-$ and $Leu_3 \cdot Cl^-$ were used to generate starting structures for the brominated and iodated peptide complexes by replacing the Cl atom with Br or I, respectively. Quantum-chemical calculations for each peptide with Br^- and I^- adducted were performed with the B3LYP density functional and the 6-31+G** basis set for each atom except Br and I, for which the CRENBL basis set and effective core potential were used. Simulated spectra were generated using harmonic frequencies scaled by a factor of 0.975 and convolved with a full width half maximum (fwhm) Gaussian profile of 40 cm^{-1} [40,42].

2.2. Experimental

All experimental spectra were measured using a 4.7 T Fourier-transform ion cyclotron resonance (FT/ICR) mass spectrometer coupled with a free electron laser (FELIX), which generates tunable infrared radiation between 900 and 1900 cm^{-1} [49]. A description of the instrument and experimental parameters is given elsewhere [50]. The halidated peptide complexes were generated by electrospray ionization with methanol/water (~85/15) solvent and flow rates of 5–10 μL min^{-1}. Solutions of peptides with sodium halide salts were prepared at 1–2 mM concentrations for both components. Ions are accumulated for ~5 s in a hexapole linear trap for collisional and radiative cooling prior to injection into the mass spectrometer. Ions that are trapped in the ion cell of the mass spectrometer are isolated with a stored waveform inverse Fourier-transform before they are irradiated by photons from FELIX (typically for ~3 s). First order rate constants are calculated from the precursor and product abundances and are corrected for frequency dependent variations in laser power [51].

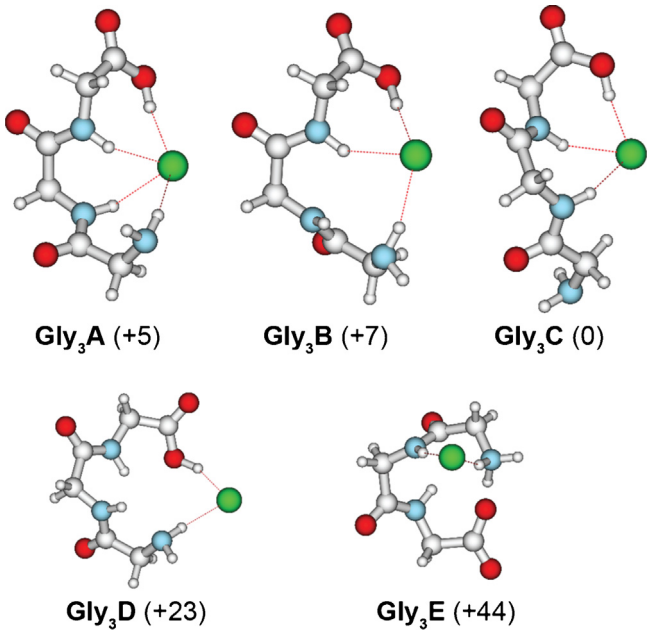

Fig. 1. Low-energy structures for $Gly_3 \cdot Cl^-$ (top) and lowest-energy structures of the endo carboxylic acid and zwitterionic forms (bottom) calculated at the B3LYP/6-31+G** level of theory (relative 298 K Gibbs free energy in kJ mol^{-1}).

3. Results and discussion

3.1. Calculated structures and relative Gibbs free energies (298 K)

3.1.1. *$Gly_3 \cdot Cl^-$*

The binding motifs of model aliphatic tripeptides to Cl^- were investigated at the B3LYP/6-31+G** level of theory. The three lowest-energy structures for $Gly_3 \cdot Cl^-$ are shown at the top of Fig. 1 (**Gly_3A–C**). The anion can coordinate to Gly_3 through hydrogen bonds (HBs) with the amides, carboxylic acid or the N-terminus. In the lowest-energy structure, **Gly_3C**, Cl^- hydrogen bonds to the two amide H atoms as well as the carboxylic acid, and the N-terminus forms a HB to the adjacent amide carbonyl O atom. In **Gly_3B** (+7 kJ mol^{-1} in Gibbs free energy at 298 K), a HB with an amide H atom is displaced by a HB with the N-terminus. A fourth HB to Cl^- (**Gly_3A**, +5 kJ mol^{-1}) does not result in additional stabilization. These results indicate that Gly_3 forms at least three HBs to Cl^-, and that any energy gained by forming a fourth HB to the anion is similar to that of forming an intramolecular HB.

The carboxylic acid groups in **Gly_3A–C** are in an exo conformation, where the acidic H atom is *trans* relative to the carbonyl O atom. The lowest-energy structure with an endo carboxylic acid, **Gly_3D**, in which the acidic H atom is *cis* relative to the carbonyl O atom, has only two HBs to Cl^- via the N- and C-termini. This structure is 23 kJ mol^{-1} higher in Gibbs free energy compared to the lowest-energy exo structure. Endo structures with a greater number of HBs to Cl^- were even higher in energy, and these results suggest that it is unfavorable for $Gly_3 \cdot Cl^-$ to adopt a structure with an endo carboxylic acid.

Structures in which Gly_3 is zwitterionic were also investigated, and the lowest-energy zwitterionic structure (**Gly_3E**) is cyclic, where both Cl^- and the carboxylate interact with the protonated N-terminus. **Gly_3E** is 44 kJ mol^{-1} higher in Gibbs free energy than **Gly_3C**, indicating that zwitterionic structures are unfavorable compared to charge-solvated structures. Based on the calculated energies, $Gly_3 \cdot Cl^-$ is likely to adopt a charge-solvated exo structure. The energy differences between **Gly_3A–C** are relatively small, indicating all three structures may exist at room temperature.

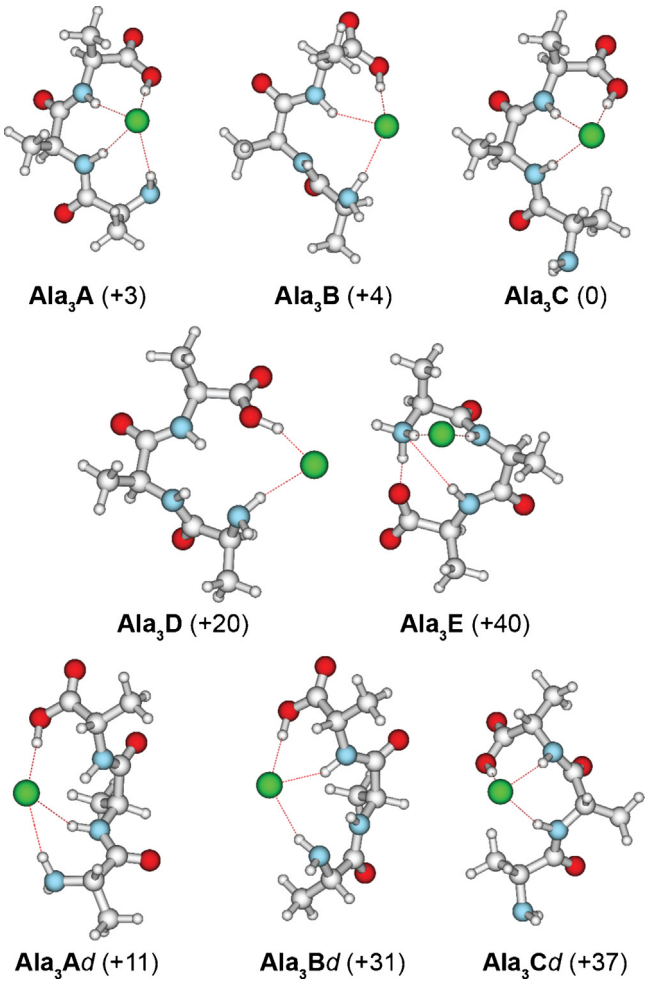

Fig. 2. Low-energy structures for $Ala_3 \cdot Cl^-$ (top), lowest-energy structures of the endo carboxylic acid and zwitterionic forms (middle) as well as diastereoisomers of low-energy structures (bottom) calculated at the B3LYP/6-31+G** level of theory (relative 298 K Gibbs free energy in kJ mol^{-1}).

Low-energy structures reported for $Gly_3 \cdot Na^+$ [39,40] are similar to those found for $Gly_3 \cdot Cl^-$, but the coordination of the peptide to the corresponding ion is "inverted." The peptide coordinates to Cl^- via HBs, whereas Na^+ coordinates to the lone pairs of the carbonyl O atoms and the N-terminus. In this respect, **Gly_3A** and **Gly_3C** are "inversions" of low-energy structures GGG-Na^+*1* and GGG-Na^+*3*, respectively, previously reported by Balaj et al. [39]. As is the case for Gly_3Cl^-, three-coordinate structures for $Gly_3 \cdot Na^+$ are lower in energy than those that are four-coordinate.

3.1.2. ***$Ala_3 \cdot Cl^-$***

To determine the effect of side chain size on anion coordination, low-energy structures for $Ala_3 \cdot Cl^-$ and their relative Gibbs free energies at 298 K (Fig. 2, top) were calculated. The hydrogen-bonding motifs and relative energies for **Ala_3A–C** are similar to those for **Gly_3A–C**, respectively. **Ala_3C** is lowest in energy, but **Ala_3A** and **Ala_3B** are energetically competitive (within 4 kJ mol^{-1}). **Ala_3D**, the lowest-energy endo structure, and **Ala_3E**, the lowest-energy zwitterionic structure, (Fig. 2, middle) are 20 and 40 kJ mol^{-1}, respectively, higher in Gibbs free energy than **Ala_3C**. Based on the calculated relative energies for $Ala_3 \cdot Cl^-$ and $Gly_3 \cdot Cl^-$, both complexes adopt similar structures, indicating that the larger side chain has little effect on anion coordination to Ala_3. As was the case for $Gly_3 \cdot Cl^-$, low-energy structures for $Ala_3 \cdot Cl^-$ are "inverted"

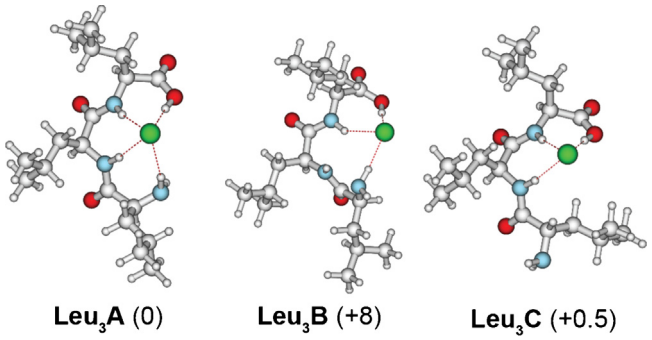

Fig. 3. Structures for $Leu_3 \cdot Cl^-$ calculated at the B3LYP/6-31+G** level of theory (relative 298 K Gibbs free energy in kJ mol^{-1}). Initial geometries for $Leu_3 \cdot Cl^-$ were generated by side chain substitution for the three lowest-energy structures of $Ala_3 \cdot Cl^-$.

compared to those for Ala_3 with Na^+ and other alkali ion adducts [39,40].

The anion in $Ala_3 \cdot Cl^-$ is a stereocenter, where the HBs between Cl^- and the peptide are analogous to covalent bonds. Initial geometries for diastereoisomers of **Ala_3A–C** were formed by changing the chirality of the anion. Geometry optimizations were performed, resulting in structures **Ala_3A*d*–C*d*** (Fig. 2, bottom). **Ala_3A*d*** is only 11 kJ mol^{-1} higher in energy compared to the lowest-energy structure (**Ala_3C**), whereas **Ala_3B*d*** and **Ala_3C*d*** are >30 kJ mol^{-1} higher in energy compared to **Ala_3C**. Thus, it is unlikely that **Ala_3B*d*** and **Ala_3C*d*** have significant contributions to the ion population. The relative enthalpies of low-energy structures for $Ala_3 \cdot Na^+$ and their diastereoisomers are within $\leq$10 kJ mol^{-1} of each other [39]. The high relative Gibbs free energies for **Ala_3B*d*** and **Ala_3C*d*** are due to the steric interactions between the methyl side chains and the amide O atoms. In contrast, the analogous steric effect for $Ala_3 \cdot Na^+$ is between the methyl groups and the relatively small amide H atoms.

3.1.3. ***$Leu_3 \cdot Cl^-$***

Low-energy structures for $Ala_3 \cdot Cl^-$ (**Ala_3A–C**) were modified to create initial geometries for $Leu_3 \cdot Cl^-$ by changing the side chain. The resulting structures for $Leu_3 \cdot Cl^-$ only change slightly upon geometry optimization (**Leu_3A–C**, Fig. 3) and maintain the same structural motifs as $Gly_3 \cdot Cl^-$ and $Ala_3 \cdot Cl^-$. **Leu_3A** and **Leu_3C** are essentially isoenergetic, and **Leu_3B** is 8 kJ mol^{-1} higher in Gibbs free energy (298 K). In summary, these results indicate that increasing steric hindrance of the alkyl side chains does not significantly change the relative energies or hydrogen-bonding motifs of low-energy structures for these complexes.

3.2. *Spectroscopy of chloridated tripeptides*

IR photodissociation of $Gly_3 \cdot Cl^-$, $Ala_3 \cdot Cl^-$ and $Leu_3 \cdot Cl^-$ results in the formation of the deprotonated tripeptide by loss of HCl as well as fragmentation to form the deprotonated amino acid. The IRMPD spectrum of each complex was measured from 1000 to 1850 cm^{-1} (Fig. 4). There are four features in the region between 1500 and 1800 cm^{-1} at ~1520, ~1625, ~1690, and ~1760 cm^{-1} with frequencies close to bands reported for Li^+, Na^+, K^+ and Cs^+ adducted to Gly_3 and Ala_3 [39–41]. The band near 1760 cm^{-1} corresponds to the carbonyl stretch of the C-terminus [28,31,32,37,39–42,52]. The bands that occur near 1520 and 1690 cm^{-1} correspond to the amide II (N—H bends) and I (carbonyl C=O stretch) vibrational modes, respectively [39–41]. The absence of an asymmetric stretch of a carboxylate group near 1650 cm^{-1} indicates that there is not a significant zwitterionic population [26–28,31–38,42], consistent with a ~40 kJ mol^{-1} higher Gibbs free energy calculated for the

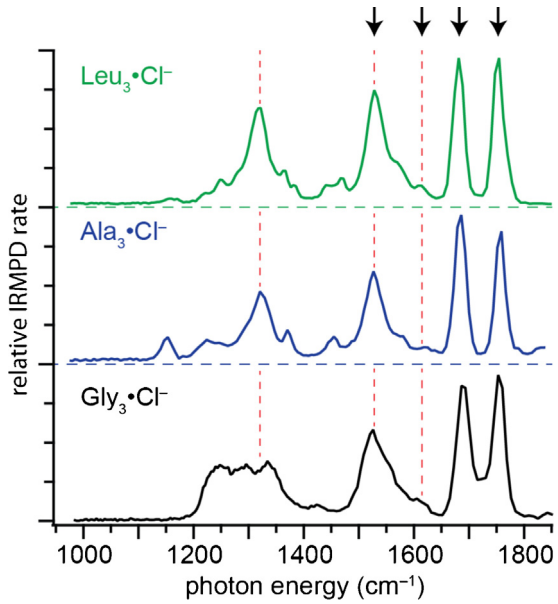

Fig. 4. IRMPD spectra of $Gly_3 \cdot Cl^-$, $Ala_3 \cdot Cl^-$, and $Leu_3 \cdot Cl^-$ at 298 K. Arrows indicate features corresponding to the amide II (N—H bends), N-terminal NH_2 scissor, amide I (C=O stretch), and C-terminal C=O stretch vibrational modes near 1520, 1625, 1690, and 1760 cm^{-1}, respectively. Horizontal dashed lines indicate a vertical offset. Vertical dashed lines serve as a guide for the eye.

zwitterionic forms of $Gly_3 \cdot Cl^-$ and $Ala_3 \cdot Cl^-$. The amide I band as well as the NH_2 scissor mode at ~1625 cm^{-1} could overlap with the carboxylate asymmetric stretch and obscure contributions from a minor population of zwitterionic structures.

Spectra of $Glu \cdot X^-$ (X = Cl, Br, I) [42] have relatively strong absorptions near 1375 cm^{-1} corresponding to the hydroxyl O—H bends of the carboxylic acid of the side chain and the C-terminus. For $Ala_3 \cdot Cl^-$ and $Leu_3 \cdot Cl^-$, the only band of comparable intensity in this region of the spectrum is at ~1325 cm^{-1}, indicating that this feature corresponds to the hydroxyl O—H bend of the C-terminal carboxylic acid. Although there is a band at 1329 cm^{-1} in the spectrum of $Gly_3 \cdot Cl^-$, there are also bands of comparable intensity at 1243 and 1285 cm^{-1}. For $Gly_3 \cdot Na^+$, a broad feature was observed by Balaj et al. at 1160 cm^{-1} that corresponds to the C-terminal carboxylic acid O—H bend, whereas bands for N—H and CH_2 bends occur from 1210 to 1290 cm^{-1} [39]. A large shift in the hydroxyl O—H bend is expected between the spectra of $Gly_3 \cdot Cl^-$ and $Gly_3 \cdot Na^+$ due to the difference in frequency of this mode for an exo vs. endo carboxylic acid whereas the N—H and CH_2 bends are expected to shift only slightly. Thus, the band for $Gly_3 \cdot Cl^-$ at 1329 cm^{-1} is likely the hydroxyl in-plane O—H bend, and the bands at 1243 and 1285 cm^{-1} are attributed to N—H and CH_2 bending modes.

3.3. Comparisons between experimental and calculated spectra

3.3.1. $Gly_3 \cdot Cl^-$

The IRMPD spectrum and calculated spectra for low-energy structures of $Gly_3 \cdot Cl^-$ are shown in Fig. 5. The carbonyl C=O stretches of the C-terminus occur near 1750 cm^{-1} for **Gly_3A–D**, in good agreement with the band at 1754 cm^{-1} in the IRMPD spectrum. In contrast, the calculated spectrum of **Gly_3E** has a carboxylate asymmetric stretch that occurs near 1650 cm^{-1}. The hydroxyl O—H bend is calculated to occur at ~1325 cm^{-1} for structures with an exo carboxylic acid (**Gly_3A–C**), in good agreement with the band in the IRMPD spectrum at 1329 cm^{-1}. This vibrational mode for an endo carboxylic acid (**Gly_3D**) is at ~1160 cm^{-1}, a region where no significant dissociation occurs. Neither spectra for **Gly_3D** nor **Gly_3E** are a good match to the IRMPD spectrum.

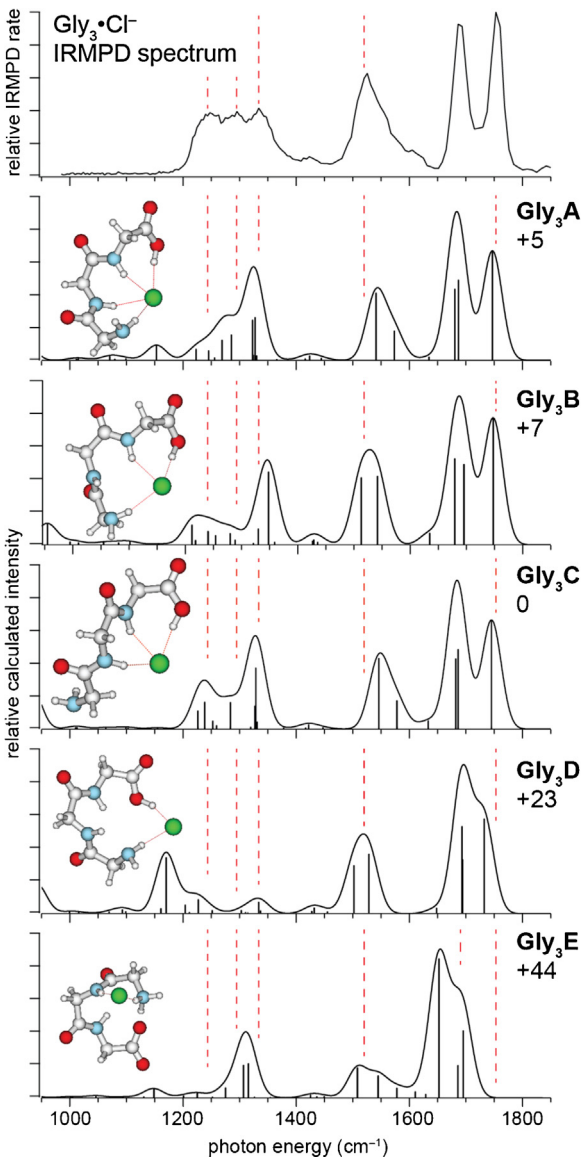

Fig. 5. Comparison of the IRMPD and calculated spectra for $Gly_3 \cdot Cl^-$. All calculations were performed at the B3LYP/6-31+G** level of theory and differences in Gibbs free energies (at 298 K) are in kJ mol^{-1}.

The calculated spectra for **Gly_3A–C** are similar, having only subtle differences that reflect only slight changes in the coordination of Cl^- to the peptide. For **Gly_3A** and **Gly_3C**, the amide N—H bends couple, resulting in a relatively intense band near 1550 cm^{-1} and a weaker band near 1575 cm^{-1}. In contrast, the coupled N—H bends for **Gly_3B** are calculated to be between 1500 and 1550 cm^{-1} and have similar intensities. The relative intensities for **Gly_3A** and **Gly_3C** are more similar to the peak at 1523 cm^{-1} in the measured spectrum, which has a shoulder at ~1560 cm^{-1}, but the calculated bands are at slightly higher frequency compared to both **Gly_3B** and the measured spectrum. The calculated spectra for **Gly_3A–C** also have bands corresponding to backbone CH_2 twists and scissor modes near the same frequencies as the bands at 1243 and 1421 cm^{-1}, respectively, in the IRMPD spectrum. There are several coupled backbone vibrations with calculated frequencies near 1300 cm^{-1}, which overlap well with the feature at ~1285 cm^{-1} in the measured spectrum. The calculated spectra for **Gly_3A** and **Gly_3C** are most consistent with the IRMPD spectrum, but contributions from **Gly_3B** cannot be ruled out. These results indicate that it is likely that all three structures are present in the ion population.

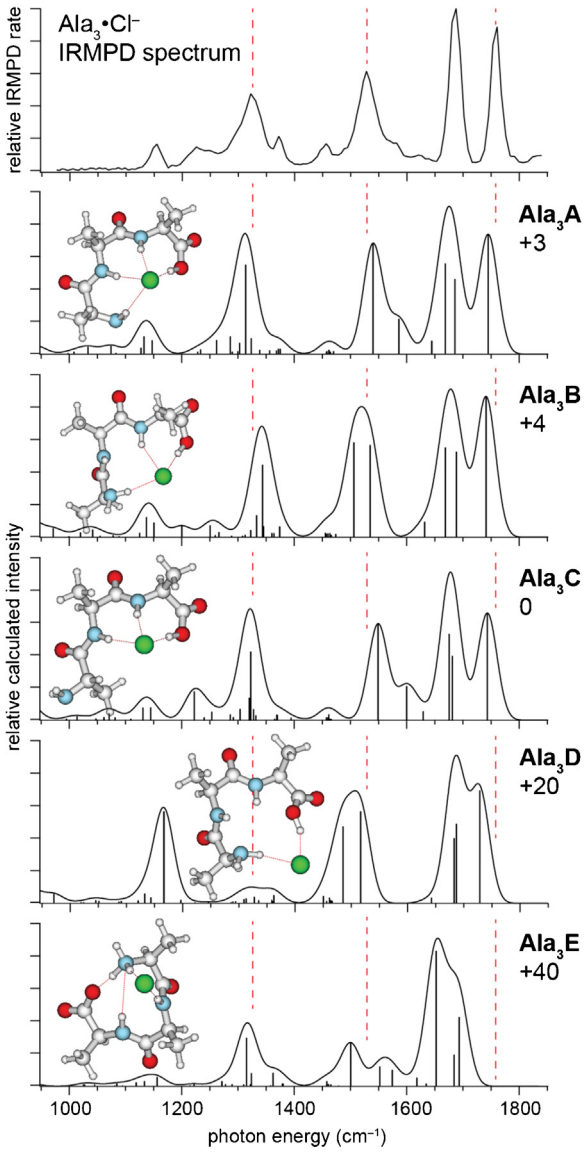

Fig. 6. Comparison of the IRMPD and calculated spectra for $Ala_3 \cdot Cl^-$. All calculations were performed at the B3LYP/6-31+G** level of theory and differences in Gibbs free energies (at 298 K) are in kJ mol^{-1}.

3.3.2. $Ala_3 \cdot Cl^-$

As was the case with $Gly_3 \cdot Cl^-$, the C-terminal carbonyl C=O stretches of charge-solvated structures for $Ala_3 \cdot Cl^-$ are calculated to occur near 1750 cm^{-1}, in good agreement with the band at 1759 cm^{-1} in the IRMPD spectrum (Fig. 6). In contrast, there is no feature near 1650 cm^{-1} of comparable intensity to the carboxylate asymmetric stretch calculated for **Ala_3E**. The hydroxyl O—H bend of the C-terminus is calculated for **Ala_3A** and **Ala_3C** to be at 1315 and 1324 cm^{-1}, respectively, in good agreement with the band at 1322 cm^{-1} in the IRMPD spectrum. The corresponding band in **Ala_3B** (1344 cm^{-1}) is slightly higher in frequency. The observed band at 1153 cm^{-1} is assigned to the methyl rocking motions, which are calculated to occur near 1150 cm^{-1}. This feature potentially overlaps with the O—H bend of an endo carboxylic acid calculated to be at ~1170 cm^{-1} for **Ala_3D**, obscuring potential contributions from this structure. Methyl umbrella and scissor motions also occur near 1375 and 1425 cm^{-1}, respectively, for each structure, and are in good agreement with the bands that appear near these frequencies in the IRMPD spectrum. The spectra of **Ala_3A** and **Ala_3C** most closely match the measured spectrum, although contributions from **Ala_3B** cannot be ruled out. In contrast, **Ala_3D** and **Ala_3E** are unlikely to have significant populations based on both calculated energies and poor match to the IRMPD spectrum.

3.3.3. $Leu_3 \cdot Cl^-$

Calculated spectra for **Leu_3A–C** (Fig. 7) each contain relatively intense bands corresponding to the hydroxyl O—H bend, the amide N—H bends, amide C=O stretch, and the C-terminal C=O stretch near 1300, 1550, 1675 and 1750 cm^{-1}, respectively. These calculated frequencies are in good agreement with the bands in the IRMPD spectrum (Fig. 7), but **Leu_3A** and **Leu_3C** are in better agreement than **Leu_3B**. The relative energies of **Leu_3A** and **Leu_3C** are nearly the same, indicating that both structures likely contribute to the ion population, but contributions from **Leu_3B** cannot be ruled out. The calculated vibrational modes of the side chain methyl groups are near 1375 and 1425 cm^{-1}. The IRMPD spectrum has two bands at ~1375 and another two centered at ~1425 cm^{-1}, and these are likely due to the coupling between the two methyl groups of each side chain.

3.4. IRMPD spectra and calculations for $Gly_3 \cdot X^-$, $Ala_3 \cdot X^-$, and $Leu_3 \cdot X^-$ (X = Cl, Br, and I)

The coordination of an ion adduct to an amino acid [30–37] or peptide [22,23,38] can depend on ion size. IRMPD spectra for $Gly_3 \cdot X^-$, where X = Cl, Br, and I, are nearly identical in the region from 1200 to 1400 cm^{-1}, and each spectrum has analogous bands between 1400 and 1900 cm^{-1}, albeit with slight shifts in frequency with changing halide anion size (Fig. 8, left). The NH_2 scissor and C-terminal carbonyl C=O bands appear at 1631 and 1768 cm^{-1}, respectively, for $Gly_3 \cdot I^-$ and are shifted to the blue by ~20 and ~15 cm^{-1}, respectively, compared to the corresponding band frequencies measured for $Gly_3 \cdot Cl^-$. In contrast, the amide N—H bends are red shifted by ~5 cm^{-1} from Gly_3Cl^- (1520 cm^{-1}) to $Gly_3 \cdot I^-$ (1515 cm^{-1}). This change in frequency is subtle, but it is also observed for $Ala_3 \cdot X^-$ and $Leu_3 \cdot X^-$ (Fig. 8, middle and right). In addition, there is a red shift in the corresponding feature for $Ala_3 \cdot M^+$ with increasing ion adduct size [40], though the change in frequency is greater for cationized vs. anionized Ala_3. The amide carbonyl C=O stretch (1691 cm^{-1}) and the backbone CH_2 bends (1421 cm^{-1}) for $Gly_3 \cdot X^-$ do not change with anion size.

There are subtle shifts in the N—H bends and the C-terminal carbonyl C=O stretch frequencies in the calculated spectra of **Gly_3A–C** with the different anions (Fig. S1), in good agreement with the IRMPD spectra. In contrast, the NH_2 scissor mode is calculated to red shift with increasing halide anion size whereas this band blue shifts in the measured spectra, and this discrepancy is not clearly understood. The similarities between the IRMPD spectra for $Gly_3 \cdot X^-$ indicate that all three complexes adopt similar conformations, and that the anion size does not significantly affect the structure of the complex. **Gly_3A–C** have similar Gibbs free energies for each of the different anions (Table 1), and the calculated spectra of **Gly_3A** and **Gly_3C** are most consistent with the corresponding measured spectra, although all three structures could likely exist for $Gly_3 \cdot X^-$.

As was the case for $Gly_3 \cdot X^-$, the spectra for $Ala_3 \cdot X^-$ and $Leu_3 \cdot X^-$ for the same peptide are similar, indicating that conformations adopted by Ala_3 and Leu_3 do not change substantially with the size of the anion adduct. The calculated spectra of structures **A** and **C** for Ala_3 and Leu_3 with the different anions (Figs. S2 and S3, respectively) are in best agreement with the corresponding IRMPD spectrum, although contributions from structure **B** cannot be ruled out. There are only minor shifts in band frequencies (<30 cm^{-1}) with anion size in the measured spectra. The N-terminal NH_2 scissor motion and the C-terminal C=O stretch features shift to higher frequencies going from Cl^- to I^- whereas the amide N—H bends

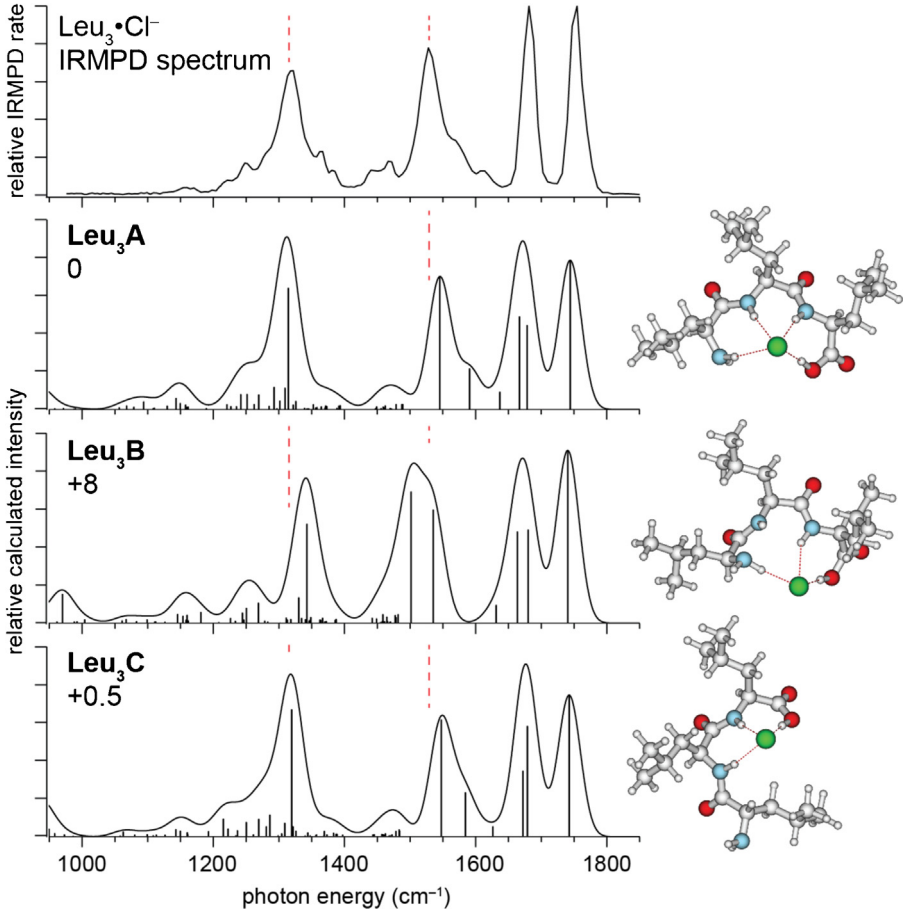

Fig. 7. Comparison of the IRMPD and calculated spectra for $Leu_3 \cdot Cl^-$. All calculations were performed at the B3LYP/6-31+G** level of theory and differences in Gibbs free energies (at 298 K) are in kJ mol^{-1}.

move to lower frequencies as the anion size increases. Similar shifts with increasing halide anion size occur in the calculated spectra for **Ala_3A–C** and **Leu_3A–C** for the amide N—H bends and the C-terminal C=O stretch, but the opposite trends occur for the NH_2 scissor modes between the calculated and the measured spectra.

Shifts in band frequencies with anion size can be attributed to either a charge transfer or Stark effect. Charge transfer can occur because the anion donates electron density to a nearby bond, which results in a change in bond strength. The vibrational frequencies of these bonds can either blue or red shift from an unperturbed oscillator depending on the orbital into which the electron density is donated [53–55], and the extent of charge transfer depends on the anion size. The electric field of an ion can extend to long distances and can also change the vibrational frequencies of functional groups remote from the ion, i.e., a Stark shift. This effect has been observed for the O—H oscillators of water molecules at the surface of hydrated ions [56,57] as well as the carbonyl C=O stretch for halidated Glu [42].

For Gly_3, Ala_3, and Leu_3 bound to Cl^-, the C-terminal C=O stretch frequency is red shifted from the corresponding band for neutral acetic acid (~1780 cm^{-1}) [58]. Anions coordinated to amino acids and peptides are closer to the carbonyl C atom than the O atom, and this arrangement results in the favorable alignment of the dipole moment of the carbonyl C=O bond and the anion's electric field. This favorable alignment causes a Stark shift in the C=O stretch frequency, which results in a red shift compared to the frequency

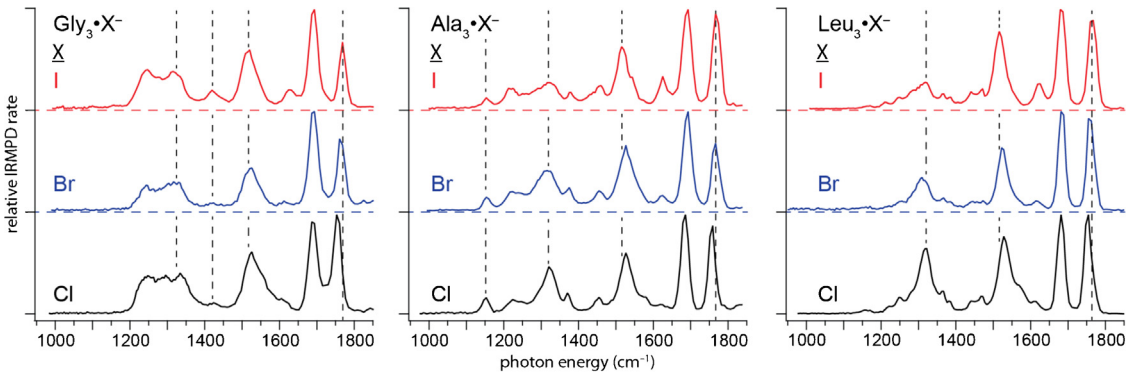

Fig. 8. IRMPD spectra (298 K) of $Gly_3 \cdot X^-$, $Ala_3 \cdot X^-$, and $Leu_3 \cdot X^-$, where X = Cl, Br, and I. Horizontal dashed lines indicate a vertical offset.

Table 1
Calculated relative Gibbs free energies (298 K) in kJ mol^{-1} for low-energy structures of $Gly_3 \cdot X^-$, $Ala_3 \cdot X^-$, and $Leu_3 \cdot X^-$, where X = Cl, Br, and I. All calculations were performed with the B3LYP functional. The CRENBL effective core potential and basis set were used for Br and I, and the 6-31+G** basis was used for all other elements.

	Cl^-	Br^-	I^-
Gly_3A	+5	+3	0
Gly_3B	+7	+5	+3
Gly_3C	0	0	+2
Ala_3A	+3	+4	+3
Ala_3B	+4	+7	+3
Ala_3C	0	0	0
Leu_3A	0	+6	+6
Leu_3B	+8	+5	+5
Leu_3C	+0.5	0	0

of an unperturbed oscillator [42,56,57]. As the size of the anion adduct increases, contributions from the Stark effect diminish and the frequency of the C=O stretch approaches that of neutral acetic acid, i.e., there is a blue shift with increasing anion size. The extent to which a charge transfer or Stark effect contribute to these shifts is unknown.

The N-terminus in structures **A** and **B** for Gly_3, Ala_3, and Leu_3 donates a HB to the anion adduct such that there is favorable alignment between the dipole of the amine N—H bonds and the anion's electric field. A Stark effect would result in a blue shift in the frequency of the NH_2 scissor mode with increasing ion size for these structures, consistent with experimental spectra. In contrast, the N-terminus in **Gly_3C**, **Ala_3C**, and **Leu_3C** is oriented such that the dipole of the amine N—H bonds and the anion's electric field are unfavorably aligned, which would result in a red shift with increasing ion size. Because structures **A** and **C** are both likely to be present, the shift in the NH_2 scissor normal mode is likely due to a charge transfer effect.

The dipoles of the amide N—H bonds are favorably aligned with the anion's electric field for **Gly_3A–C**, **Ala_3A–C**, and **Leu_3A–C**. The features corresponding to the amide N—H bends shift to lower frequencies with increasing ion size, but this trend opposite to what would be expected for a Stark shift. Thus, the change in frequency of these vibrational modes can only be attributed to the charge transfer effect.

4. Conclusion

IRMPD spectra were measured for $Gly_3 \cdot X^-$, $Ala_3 \cdot X^-$ and $Leu_3 \cdot X^-$ (where X = Cl, Br and I). For each peptide, spectra appear nearly identical, albeit with slight differences in frequency for some spectral features, indicating that each peptide adopts similar conformations that do not depend significantly on anion size. These results are also supported by theory. Comparisons between measured spectra and those calculated for low-energy structures of Cl^- adducted to Gly_3, Ala_3 and Leu_3 indicate that all three complexes adopt the same binding motifs and that the size of the alkyl size chain has little influence on coordination patterns. Low-energy structures for $Gly_3 \cdot X^-$ and $Ala_3 \cdot X^-$ are "inverted" compared to those for $Gly_3 \cdot Na^+$ and $Ala_3 \cdot M^+$ (M = Li, Na, K, Cs), respectively [39,40]. The "inversion" in coordination between $Ala_3 \cdot M^+$ and $Ala_3 \cdot X^-$ results in greater steric hindrance for some structures for the latter. The bands for the C-terminal C=O stretch blue shift with increasing size of the anion adduct whereas the amide N—H bend features red shift as the size of the ion adduct increases. The former is consistent with contributions from both Stark and charge transfer effects whereas the latter can only be explained by the charge transfer effect. These results provide insight into anion-peptide interactions and whether or not steric effects due to the alkyl groups of aliphatic amino acids influence halide coordination.

Supporting information

Calculated spectra for low-energy structures for $Gly_3 \cdot X^-$, Ala_3X^- and Leu_3X^- (X = Cl, Br and I), can be found in supporting information.

Acknowledgements

IRMPD spectra were measured at the FOM Institute for Plasma Physics "Rijnhuizen", which is financially supported by the Nederlandse Organisatie voor Wetenschappelijk Onderzoek (NWO). The authors thank Dr. Britta Redlich and the rest of the FELIX staff for excellent support as well as the University of California, Berkeley Molecular Graphics and Computation Facility (CHE-0840505). Generous financial support was provided by the National Science Foundation (Grants CHE-1306720 and OISE-730072).

Appendix A. Supplementary data

Supplementary data associated with this article can be found, in the online version, at http://dx.doi.org/10.1016/j.ijms.2014.02.019.

References

[1] M. Chesler, Regulation and modulation of pH in the brain, Physiol. Rev. 83 (2003) 1183–1221.
[2] J.M. Russell, W.F. Boron, Role of chloride transport in regulation of intracellular pH, Nature 264 (1976) 73–74.
[3] J.A. Loo, Studying noncovalent protein complexes by electrospray ionization mass spectrometry, Mass Spectrom. Rev. 16 (1997) 1–23.
[4] A.M. Pyle, Metal ions in the structure and function of RNA, J. Biol. Inorg. Chem. 7 (2002) 679–690.
[5] S.G. Dashper, L. Brownfield, N. Slakeski, P.S. Zilm, A.H. Rogers, E.C. Reynolds, Sodium ion-driven serine/threonine transport in *Porphyromonas gingivalis*, J. Bacteriol. 183 (2001) 4142–4148.
[6] S. Frings, D. Reuter, S.J. Kleene, Neuronal Ca^{2+}-activated Cl^- channels – homing in on an elusive channel species, Prog. Neurobiol. 60 (2000) 247–289.
[7] S.J. Kleene, R.C. Gesteland, Calcium-activated chloride conductance in frog olfactory cilia, J. Neurosci. 11 (1991) 3624–3629.
[8] S. Firestein, G.M. Shepherd, Interaction of anionic and cationic currents leads to a voltage dependence in the odor response of olfactory receptor neurons, J. Neurophysiol. 73 (1995) 562–567.
[9] R.J. Delay, A.E. Dubin, V.E. Dionne, A cyclic nucleotide-dependent chloride conductance in olfactory receptor neurons, J. Membr. Biol. 159 (1997) 53–60.
[10] M. Hallani, J.W. Lynch, P.H. Barry, Characterization of calcium-activated chloride channels in patches excised from the dendritic knob of mammalian olfactory receptor neurons, J. Membr. Biol. 161 (1998) 163–171.
[11] R.A. Jockusch, W.D. Price, E.R. Williams, Structure of cationized arginine (Arg·M^+, M = H, Li, Na, K, Rb, and Cs) in the gas phase: further evidence for zwitterionic arginine, J. Phys. Chem. A 103 (1999) 9266–9274.
[12] B.A. Cerda, L. Cornett, C. Wesdemiotis, Probing the interaction of alkali and transition metal ions with bradykinin and its des-arginine derivatives via matrix-assisted laser desorption/ionization and postsource decay mass spectrometry, Int. J. Mass Spectrom. 193 (1999) 205–226.
[13] B.A. Cerda, C. Wesdemiotis, Zwitterionic vs. charge-solvated structures in the binding of arginine to alkali metal ions in the gas phase, Analyst 125 (2000) 657–660.
[14] F. Rogalewicz, Y. Hoppilliard, G. Ohanessian, Fragmentation mechanisms of α-amino acids protonated under electrospray ionization: a collisional activation and *ab initio* theoretical study, Int. J. Mass Spectrom. 195 (2000) 565–590.
[15] J.M. Farrugia, R.A.J. O'Hair, Involvement of salt bridges in a novel gas phase rearrangement of protonated arginine-containing dipeptides which precedes fragmentation, Int. J. Mass Spectrom. 222 (2003) 229–242.
[16] P.Y.I. Shek, J.F. Zhao, Y. Ke, K.W.M. Siu, A.C. Hopkinson, Fragmentations of protonated arginine, lysine and their methylated derivatives: concomitant losses of carbon monoxide or carbon dioxide and an amine, J. Phys. Chem. A 110 (2006) 8282–8296.
[17] T. Wyttenbach, M.T. Bowers, Gas-phase conformations: the ion mobility/ion chromatography method, in: C.A. Schalley (Ed.), Modern Mass Spectrometry, Springer-Verlag, Berlin, 2003, pp. 207–232.
[18] L.J. Han, S.J. Hyung, J.J.S. Mayers, B.T. Ruotolo, Bound anions differentially stabilize multiprotein complexes in the absence of bulk solvent, J. Am. Chem. Soc. 133 (2011) 11358–11367.
[19] S.I. Merenbloom, T.G. Flick, M.P. Daly, E.R. Williams, Effects of select anions from the Hofmeister series on the gas-phase conformations of protein ions measured with traveling-wave ion mobility spectrometry/mass spectrometry, J. Am. Soc. Mass Spectrom. 22 (2011) 1978–1990.

[20] M.S. Glover, J.M. Dilger, F. Zhu, D.E. Clemmer, The binding of Ca^{2+}, Co^{2+}, Ni^{2+}, Cu^{2+}, and Zn^{2+} cations to angiotensin I determined by mass spectrometry based techniques, Int. J. Mass Spectrom. 354-355 (2013) 318–325.
[21] A. Kamariotis, O.V. Boyarkin, S.R. Mercier, R.D. Beck, M.F. Bush, E.R. Williams, T.R. Rizzo, Infrared spectroscopy of hydrated amino acids in the gas phase: protonated and lithiated valine, J. Am. Chem. Soc. 128 (2006) 905–916.
[22] R.C. Dunbar, N.C. Polfer, G. Berden, J. Oomens, Metal ion binding to peptides: oxygen or nitrogen sites? Int. J. Mass Spectrom. 330 (2012) 71–77.
[23] R.C. Dunbar, J. Oomens, G. Berden, J.K.C. Lau, U.H. Verkerk, A.C. Hopkinson, K.W.M. Siu, Metal ion complexes with HisGly: comparison with PhePhe and PheGly, J. Phys. Chem. A 117 (2013) 5335–5343.
[24] N.C. Polfer, B. Paizs, L.C. Snoek, I. Compagnon, S. Suhai, G. Meijer, G. von Helden, J. Oomens, Infrared fingerprint spectroscopy and theoretical studies of potassium ion tagged amino acids and peptides in the gas phase, J. Am. Chem. Soc. 127 (2005) 8571–8579.
[25] R.C. Dunbar, N.C. Polfer, J. Oomens, Gas-phase zwitterion stabilization by a metal dication, J. Am. Chem. Soc. 129 (2007) 14562–14563.
[26] C. Kapota, J. Lemaire, P. Maitre, G. Ohanessian, Vibrational signature of charge solvation vs salt bridge isomers of sodiated amino acids in the gas phase, J. Am. Chem. Soc. 126 (2004) 1836–1842.
[27] M.F. Bush, J. Oomens, E.R. Williams, Proton affinity and zwitterion stability: new results from infrared spectroscopy and theory of cationized lysine and analogues in the gas phase, J. Phys. Chem. A 113 (2009) 431–438.
[28] J.S. Prell, J.T. O'Brien, J.D. Steill, J. Oomens, E.R. Williams, Structures of protonated dipeptides: the role of arginine in stabilizing salt bridges, J. Am. Chem. Soc. 131 (2009) 11442–11449.
[29] J.S. Prell, T.G. Flick, J. Oomens, G. Berden, E.R. Williams, Coordination of trivalent metal cations to peptides: results from IRMPD spectroscopy and theory, J. Phys. Chem. A 114 (2010) 854–860.
[30] A.L. Heaton, V.N. Bowman, J. Oomens, J.D. Steill, P.B. Armentrout, Infrared multiple photon dissociation spectroscopy of cationized asparagine: effects of metal cation size on gas-phase conformation, J. Phys. Chem. A 113 (2009) 5519–5530.
[31] M.W. Forbes, M.F. Bush, N.C. Polfer, J. Oomens, R.C. Dunbar, E.R. Williams, R.A. Jockusch, Infrared spectroscopy of arginine cation complexes: direct observation of gas-phase zwitterions, J. Phys. Chem. A 111 (2007) 11759–11770.
[32] P.B. Armentrout, M.T. Rodgers, J. Oomens, J.D. Steill, Infrared multiphoton dissociation spectroscopy of cationized serine: effects of alkali-metal cation size on gas-phase conformation, J. Phys. Chem. A 112 (2008) 2248–2257.
[33] M.F. Bush, J. Oomens, R.J. Saykally, E.R. Williams, Effects of alkaline earth metal ion complexation on amino acid zwitterion stability: results from infrared action spectroscopy, J. Am. Chem. Soc. 130 (2008) 6463–6471.
[34] M.T. Rodgers, P.B. Armentrout, J. Oomens, J.D. Steill, Infrared multiphoton dissociation spectroscopy of cationized threonine: effects of alkali-metal cation size on gas-phase conformation, J. Phys. Chem. A 112 (2008) 2258–2267.
[35] J.T. O'Brien, J.S. Prell, J.D. Steill, J. Oomens, E.R. Williams, Interactions of mono- and divalent metal ions with aspartic and glutamic acid investigated with IR photodissociation spectroscopy and theory, J. Phys. Chem. A 112 (2008) 10823–10830.
[36] R.C. Dunbar, A.C. Hopkinson, J. Oomens, C.K. Siu, K.W.M. Siu, J.D. Steill, U.H. Verkerk, J.F. Zhao, Conformation switching in gas-phase complexes of histidine with alkaline earth ions, J. Phys. Chem. B 113 (2009) 10403–10408.
[37] M. Citir, E.M.S. Stennett, J. Oomens, J.D. Steill, M.T. Rodgers, P.B. Armentrout, Infrared multiple photon dissociation spectroscopy of cationized cysteine: effects of metal cation size on gas-phase conformation, Int. J. Mass Spectrom. 297 (2010) 9–17.
[38] J.S. Prell, M. Demireva, J. Oomens, E.R. Williams, Role of sequence in salt-bridge formation for alkali metal cationized GlyArg and ArgGly investigated with IRMPD spectroscopy and theory, J. Am. Chem. Soc. 131 (2009) 1232–1242.
[39] O.P. Balaj, C. Kapota, J. Lemaire, G. Ohanessian, Vibrational signatures of sodiated oligopeptides (GG-Na^+, GGG-Na^+, AA-Na^+ and AAA-Na^+) in the gas phase, Int. J. Mass Spectrom. 269 (2008) 196–209.
[40] R.C. Dunbar, J.D. Steill, J. Oomens, Conformations and vibrational spectroscopy of metal-ion/polylalanine complexes, Int. J. Mass Spectrom. 297 (2010) 107–115.
[41] O.P. Balaj, D. Semrouni, V. Steinmetz, E. Nicol, C. Clavaguera, G. Ohanessian, Structure of sodiated polyglycines, Chem. Eur. J. 18 (2012) 4583–4592.
[42] J.T. O'Brien, J.S. Prell, G. Berden, J. Oomens, E.R. Williams, Effects of anions on the zwitterion stability of Glu, His and Arg investigated by IRMPD spectroscopy and theory, Int. J. Mass Spectrom. 297 (2010) 116–123.
[43] J. Schmidt, S.R. Kass, Zwitterion vs neutral structures of amino acids stabilized by a negatively charged site: infrared photodissociation and computations of proline-chloride anion, J. Phys. Chem. A 117 (2013) 4863–4869.
[44] E.M. Milner, M.G.D. Nix, C.E.H. Dessent, Collision-induced dissociation of halide ion-arginine complexes: evidence for anion-induced zwitterion formation in gas-phase arginine, J. Phys. Chem. A 116 (2012) 801–809.
[45] P. Skurski, J. Rak, J. Simons, M. Gutowski, Quasidegeneracy of zwitterionic and canonical tautomers of arginine solvated by an excess electron, J. Am. Chem. Soc. 123 (2001) 11073–11074.
[46] S.J. Xu, W.J. Zheng, D. Radisic, K.H. Bowen, The stabilization of arginine's zwitterion by dipole-binding of an excess electron, J. Chem. Phys. 122 (2005) 091103.
[47] S.R. Kass, Zwitterion–dianion complexes and anion-anion clusters with negative dissociation energies, J. Am. Chem. Soc. 127 (2005) 13098–13099.
[48] Y. Shao, L.F. Molnar, Y. Jung, J. Kussmann, C. Ochsenfeld, S.T. Brown, A.T.B. Gilbert, L.V. Slipchenko, S.V. Levchenko, D.P. O'Neill, R.A. DiStasio, R.C. Lochan, T. Wang, G.J.O. Beran, N.A. Besley, J.M. Herbert, C.Y. Lin, T. Van Voorhis, S.H. Chien, A. Sodt, R.P. Steele, V.A. Rassolov, P.E. Maslen, P.P. Korambath, R.D. Adamson, B. Austin, J. Baker, E.F.C. Byrd, H. Dachsel, R.J. Doerksen, A. Dreuw, B.D. Dunietz, A.D. Dutoi, T.R. Furlani, S.R. Gwaltney, A. Heyden, S. Hirata, C.P. Hsu, G. Kedziora, R.Z. Khalliulin, P. Klunzinger, A.M. Lee, M.S. Lee, W. Liang, I. Lotan, N. Nair, B. Peters, E.I. Proynov, P.A. Pieniazek, Y.M. Rhee, J. Ritchie, E. Rosta, C.D. Sherrill, A.C. Simmonett, J.E. Subotnik, H.L. Woodcock, W. Zhang, A.T. Bell, A.K. Chakraborty, D.M. Chipman, F.J. Keil, A. Warshel, W.J. Hehre, H.F. Schaefer, J. Kong, A.I. Krylov, P.M.W. Gill, M. Head-Gordon, Advances in methods and algorithms in a modern quantum chemistry program package, Phys. Chem. Chem. Phys. 8 (2006) 3172–3191.
[49] J.J. Valle, J.R. Eyler, J. Oomens, D.T. Moore, A.F.G. van der Meer, G. von Helden, G. Meijer, C.L. Hendrickson, A.G. Marshall, G.T. Blakney, Free electron laser-Fourier transform ion cyclotron resonance mass spectrometry facility for obtaining infrared multiphoton dissociation spectra of gaseous ions, Rev. Sci. Instrum. 76 (2005) 023103.
[50] N.C. Polfer, J. Oomens, D.T. Moore, G. von Helden, G. Meijer, R.C. Dunbar, Infrared spectroscopy of phenylalanine Ag(I) and Zn(II) complexes in the gas phase, J. Am. Chem. Soc. 128 (2006) 517–525.
[51] J.S. Prell, J.T. O'Brien, E.R. Williams, IRPD spectroscopy and ensemble measurements: effects of different data acquisition and analysis methods, J. Am. Mass. Spectrom. 21 (2010) 800–809.
[52] J.D. Steill, J. Oomens, Gas-phase deprotonation of *p*-hydroxybenzoic acid investigated by IR spectroscopy: solution-phase structure is retained upon ESI, J. Am. Chem. Soc. 131 (2009) 13570–13571.
[53] S. Scheiner, Hydrogen Bonding, Oxford University Press, New York, 1997.
[54] P. Hobza, Z. Havlas, Improper, blue-shifting hydrogen bond, Theor. Chem. Acc. 108 (2002) 325–334.
[55] A.M. Wright, A.A. Howard, C. Howard, G.S. Tschumper, N.I. Hammer, Charge transfer and blue shifting of vibrational frequencies in a hydrogen bond acceptor, J. Phys. Chem. A 117 (2013) 5435–5446.
[56] J.S. Prell, J.T. O'Brien, E.R. Williams, Structural and electric field effects of ions in aqueous nanodrops, J. Am. Chem. Soc. 133 (2011) 4810–4818.
[57] J.T. O'Brien, E.R. Williams, Effects of ions on hydrogen-bonding water networks in large aqueous nanodrops, J. Am. Chem. Soc. 134 (2012) 10228–10236.
[58] Coblentz Society, Inc., Evaluated infrared reference spectra, in: P.J. Linstrom, W.G. Mallard (Eds.), NIST Chemistry WebBook, NIST Standard Reference Database Number 69, National Institute of Standards and Technology, Gaithersburg, MD, 2009, p. 20899, http://webbook.nist.Gov (retrieved 11.04.13).